Materials Science and Engineering A 545 (2012) 118–122

Contents lists available at SciVerse ScienceDirect

Materials Science and Engineering A

journal homepage: www.elsevier.com/locate/msea

Mechanical properties of fcc/fcc Cu/Nb nanostructured multilayers

J.Y. Zhang, P. Zhang, X. Zhang, R.H. Wang, G. Liu*, G.J. Zhang, J. Sun*

State Key Laboratory for Mechanical Behavior of Materials, Xi'an Jiaotong University, Xi'an 710049, PR China

ARTICLE INFO

Article history:
Received 27 July 2011
Received in revised form 3 February 2012
Accepted 2 March 2012
Available online 13 March 2012

Keywords:
Phase transition
Cu/Nb nanostructured multilayer
Mechanical properties

ABSTRACT

The phase transition of Nb from body-centered cubic (bcc) to face-centered cubic (fcc) has been found in Cu/Nb nanostructured multilayers with modulation period (λ) spanning from 5 to 300 nm, and was analyzed by using a thermodynamic model. As λ decreases, the strength of multilayers increase and approach saturation of ~2.88 GPa at a few nm layer thickness. Size dependent strengthening in present fcc/fcc Cu/Nb multilayers is explained in terms of dislocation based strengthening mechanisms. The enhanced modulus of fcc/fcc Cu/Nb is also observed.

1. Introduction

Nanostructured multilayer films (NMFs) are of interest due to the novel properties that emerge as the individual layer thickness is reduced to nanometer-scale [1–6]. As the layer thickness h_M (one half of the modulation period λ) is decreased, three different regions of hardness are frequently observed in both fcc/bcc type (such as Cu/Cr [7], Cu/Nb [8] and Al/V [9]) and fcc/fcc type (such as Cu/Ag [10] and Cu/Ni [11]) NMFs with constant modulation ratio (η) ~1: the first region shows Hall–Petch (H–P) behavior; the second region shows an even greater dependence on layer thickness; and the third region exhibits a plateau or softening of hardness. Correspondingly, three kinds of strengthening mechanisms have proposed to describe the variation in hardness/strength of these materials as their characteristic dimensions shrinking toward to the nanoregime, e.g. (i) the Hall–Petch like strengthening relationship based on dislocations pile up against the interface [1,7,12], which works at the sub-micrometer to micron length scales, (ii) the confined layer slip (CLS) mechanism involving the single dislocation loop glide confined to isolated layers [8,13,14], which is applicable at few to a few tens of nanometers length scales, and (iii) the interface barrier strength (IBS) mechanism considering single dislocation cutting cross the interface [15,16], which comes into operation at a few nanometers length scales.

Dimensionally induced structural transition in multilayers has been an area of considerable interest in nanostructured materials due to the ability to control properties by engineering the structure of materials at the nanoscale. When h_M in a multilayer is reduced to the nanoregime, it often exhibits structural transitions resulting in one or more of the layers adopting a crystal structure different from its bulk equilibrium state [17–22]. For example, in Al/Ti multilayers, with increasing λ or h_M, the Al transformed once from hexagonal close-packed (hcp) to fcc, but the Ti transformed twice: from hcp to fcc, then back to hcp [19,20]. Some models are used commonly to explain structural stabilities in multilayers, involving the influence of interfaces on bulk stacking fault energies [23], coherency strains [24] and the competition between bulk and interfacial free energies [25–27].

A question naturally arises as to how the phase transition influences the mechanical properties of NMFs such as hardness/strength and modulus. In this paper, the transition of bcc Nb to fcc structure, as well as the modulus and hardness enhancement in fcc/fcc Cu/Nb NMFs with equal h_M have been observed. We explained the phase transition on the base of thermodynamic model constructed on the competition between bulk and interfacial free energies and analyzed the unique mechanical behavior in Cu/Nb NMFs.

2. Experiment details

2.1. Sample preparation and microstructure characterization

Cu (99.995%) and Nb (99.99%) targets were used to deposit Cu/Nb NMFs on Si (1 0 0) wafer with native oxide by direct current (DC) magnetron sputtering. The chamber was evacuated to a base pressure of ~6×10^{-7} Torr, and 1.0–2.5 $\times 10^{-3}$ Torr Ar were used during deposition. The substrate was neither heated nor cooled during deposition. The constituents within the Cu/Nb NMFs have equal individual layer thickness h_M ($h_M = h_{Cu} = h_{Nb}$) varying from 2.5 to 150 nm. Prior to deposition, the substrates were firstly cleaned by Ar ion bombardment with 1 keV. The deposition rates were

* Corresponding authors.
E-mail address: lgsammer@mail.xjtu.edu.cn (G. Liu).

0921-5093/$ – see front matter © 2012 Elsevier B.V. All rights reserved.
doi:10.1016/j.msea.2012.03.009

0.6 nm/s for both Cu and Nb. The Nb layer was first deposited on the substrate and finally the most top layer of the multilayer was Cu. The total thickness of the Cu/Nb NMFs was ~600 nm. The high-angle X-ray diffraction (XRD) experiment was carried out using an improved Rigaku D/max-RB X-ray diffractometer with Cu $K_{\alpha 1}$ radiation (~0.15406 nm) and a graphite monochromator to determine the crystallographic texture and the residual stress of the Cu/Nb NMFs by using "$\sin^2\psi$ method" [28–30]. Transmission electron microscopy (TEM) observation was performed using a JEOL-2100F high-resolution transmission electron microscope (HRTEM) with an acceleration tension of 200 kV to observe the modulation structure and the interface structure. Monolithic Cu film and Nb film with thickness ~600 nm were also deposited onto Si (1 0 0) under the same condition for comparison.

2.2. Hardness test

The mechanical properties (hardness H and modulus E) tests were performed using a MTS nanoindenter XP, equipped with a Berkovich diamond indenter and patented continuous stiffness method (CSM) technique, in a constant displacement rate of 2 nm/s. The maximum indentation depth was 250 nm, with a displacement resolution of <0.01 nm and a loading resolution of 50 nN. A frequency of 45 Hz was used to avoid sensitivity to thermal drift. A minimum of 9 indents was performed on each specimen to get an average hardness value and standard deviation. Generally, a plateau is reached in the measured hardness vs. indentation depth, and then an average value of hardness is obtained. Because the thickness of the multilayers is only 600 nm, a substrate effect probably contribute to the hardness and modulus measurements. To distinguish thin film and substrate contributions in hardness measurement, an effective method is to measure the corresponding maximum load and indentation size of multilayers at different penetration depths of 100, 200, 300, 450, 600, 800 nm, then make a Mayer plot [32]. For present Cu/Nb multilayers, the log–log plot of indentation size vs. applied load reveals a transition region between the indentation depths of 300 and 450 nm. This indicates that the hardness value below 300 nm depth, the plateau value, is the intrinsic hardness of the multilayer film.

For nanoindentation the unloading is considered to be an elastic affair with no reverse plasticity. The slope of the unloading curve at any point is called the contact stiffness. The contact stiffness in conjunction with the calculated contact area provides a measurement of the reduced elastic modulus as follows:

$$E_r = \frac{\sqrt{\pi}}{2} S \frac{1}{\sqrt{A}}, \tag{1}$$

where A is the projected area of the contact area, S is the contact stiffness, and E_r is the reduced modulus expressed in terms of the elastic properties of the indenter (i) and the multilayer (m) as

$$\frac{1}{E_r} = \frac{1-\nu_i^2}{E_i} + \frac{1-\nu_m^2}{E_m}, \tag{2}$$

where E is the modulus and ν is the Poisson ratio. Eq. (1) is applicable to a thin film on a substrate only if the multilayer and substrate have the same elastic properties. If the multilayer and substrate are elastically inhomogeneous – which is the case of Cu/Nb multilayer on the Si substrate – then Eq. (1) returns the composite modulus (multilayers + substrate) because the substrate also contributes to the measured modulus E. To avoid the substrate effects on the intrinsic modulus of the Cu/Nb NMFs, we used the simple model developed by Doerner and Nix [31] to determine the elastic modulus of the multilayers from the composite modulus, following the treatment of Ref. [32]. In this model, the empirical relationship among E, E_m and E_{sb} can be expressed as:

$$\frac{1}{E} = \frac{1}{E_m} + \left(\frac{1}{E_{sb}} - \frac{1}{E_m}\right) \exp\left(-\alpha \frac{t}{h_0}\right), \tag{3}$$

where α is a constant, t is the multilayer thickness and h_0 is the penetration depth.

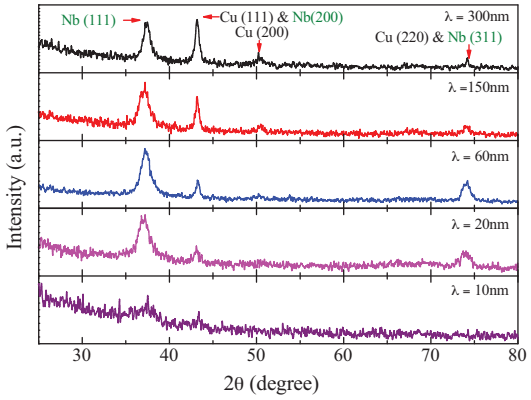

Fig. 1. The XRD spectra of Cu/Nb NMFs showing the fcc-Nb with (1 1 1) diffraction peak and the fcc-Cu with (1 1 1) and (2 0 0) diffraction peak.

3. Results and discussion

3.1. Microstructure

The X-ray diffraction (XRD) spectra for present Cu/Nb NMFs revealed both the Cu layers and Nb layers are polycrystalline structure, as shown in Fig. 1. The Cu layers exhibited a strong <1 1 1> out-of-plane texture, and diffraction peaks of Cu do not shift compared with the unstressed state, while the fcc Nb (1 1 1) peak (~36.8° at unstressed state) [33,34] shifted significantly toward to high angle (~37.1–37.3°), see Fig. 1. Moreover, it monotonically increases from 37.1° to 37.3° as the λ decreases from 300 to 5 nm. Correspondingly, the out-of-plane interplanar spacing of (1 1 1) is about 2.423–2.411 Å. These quite approach the equilibrium state fcc (1 1 1) interplanar spacing about 2.444 Å (i.e., lattice constant is about 4.233 Å), indicating interplanar spacing perpendicular to the film plane decreases with decreasing periodicity. The compressed out-of-plane interplanar spacing of fcc Nb layer is favorable for the enhanced indentation modulus, which have been found in Cu/W NMFs [32]. Owing to the distance of atomic planes of Nb (2 0 0) and (3 1 1) are respectively very close to that of Cu (1 1 1) and (2 2 0) so that their peaks overlap with each other in the XRD pattern. For the fcc/bcc Cu/Nb NMFs with Kurdjumov–Sachs (K–S) orientation relationship [5] in the growth direction: {1 1 1}Cu//{1 1 0}Nb; <1 1 0>Cu//<1 1 1>Nb, the lattice mismatch (δ) between Cu and Nb is about ~10.5%, while for the fcc/fcc Cu/Nb NMFs with cube-on-cube structure, the δ between Cu and Nb is as high as ~15.7%. In fact, the real lattice mismatch is not only proportional to the lattice constant mismatch but also depends on the specific interface structure, e.g. with or without interface intermixing layer. Thus, δ may not be determined accurately. For the sake of simplicity, δ is defined as a ratio of the lattice constant difference between the two constituent crystals to their mean value without taking account of the detailed relationship of crystallographic orientation at the interface [3]. Thus, the δ for fcc/bcc Cu/Nb NMFs is about 9.1%, while the δ for fcc/fcc ones is about 15.7%. In other words, more misfit dislocations arrange at the fcc/fcc Cu/Nb interfaces.

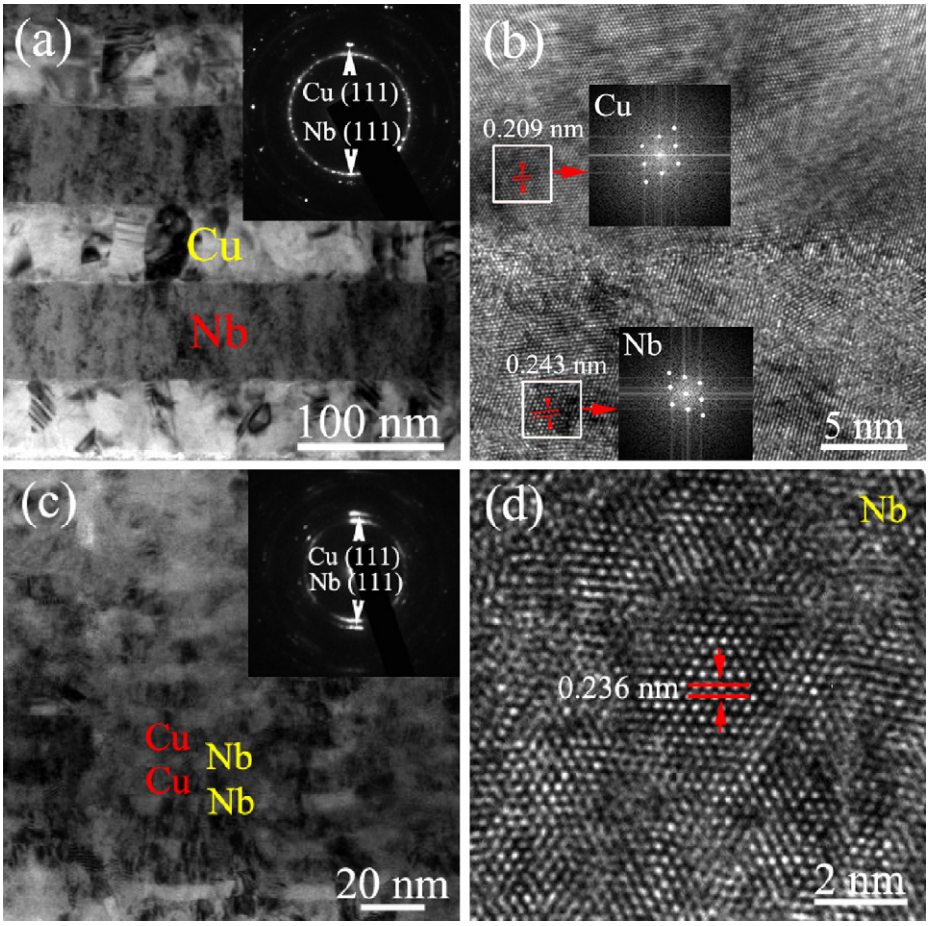

Fig. 2. Bright-field cross-sectional TEM micrograph typically showing the modulation structure of the Cu/Nb NMFs with (a) $\lambda = 150$ nm and (c) $\lambda = 20$ nm. (b) and (d) are HRTEM images typically showing the crystal structure of Cu/Nb and fcc-Nb layer. Inserts in (a) and (c) are the corresponding selected area diffraction pattern (SADP). Inserts in (b) are the FFT for Cu and Nb of the squared box area, respectively.

Cross-sectional views of the fcc/fcc Cu/Nb NMFs from the transmission electron microscopy (TEM) observations are displayed in Fig. 2, showing clear modulation structure and columnar grains in the Cu layers and ultra-fine nanocrystals in the Nb layers (see Fig. 2(a) and (c)). Some Cu grains show growth twins. The average grain sizes of both Cu and Nb scale with the layer thickness, and Cu grain size larger than that of Nb. No significant intermixing between Cu and Nb has been observed as proved by the interface HR-TEM observation shown in Fig. 2(b). Further HR-TEM examinations reveal that the interplanar spacing is about 0.244 nm, which provides the other evidence of fcc Nb rather than bcc Nb, as shown in Fig. 2(b) and (d). The selected-area diffraction patterns (SADP) of the cross-section samples are consistent with the XRD results. The phase transitions of bcc Nb to fcc Nb have also been found in the growth of Nb film due to cubic or hcp stacking of the isolated Nb atoms or the $NbCl_5$ molecules adsorbed on the substrate [34], and in nanocrystalline Nb during deformation (ball milling) owing to the stored excess energy in nanocrystalline bcc Nb [35,36], respectively.

As to the bcc to fcc phase transition of Nb, Li et al. [27] proposed a simple model for structural stability of multilayer systems based on a thermodynamic model for interface energy and the Goldschmidt premise for lattice contraction, i.e., when an fcc phase transits to a bcc phase, the corresponding atomic diameter must contract 3%, and vice versa. In this model, the corresponding difference of the interfacial energies between Nb and Cu with certain structures, $\Delta\gamma$, can be written as follows [27]:

$$\Delta\gamma = \gamma_{in} - \gamma_c = \frac{4\bar{a}\bar{S}_{vib}\bar{H}_m}{3\bar{V}_m R} - \frac{\mu_{Nb}\mu_{Cu}\bar{a}a_{Nb}}{2\pi(\mu_{Nb}+\mu_{Cu})\left|a_{Nb}-a_{Cu}\right|(1+\nu)} \times \left(\ln\left(\frac{a_{Nb}}{2\left|a_{Nb}-a_{Cu}\right|}\right)+1\right), \quad (4)$$

where γ_{in} is the incoherent interface energy for fcc/bcc Cu/Nb, γ_c is the coherent or semi-coherent interface energy for fcc/fcc Cu/Nb; $a_{Nb}(a_{Cu})$ and $\mu_{Nb}(\mu_{Cu})$ are the atomic diameter and shear modulus of Nb (Cu), respectively; $R \sim 8.314$ J/(K mol) is the ideal gas constant, $\nu \sim 0.343$ is the Poisson ratio; $\bar{a}, \bar{H}_m, \bar{S}_{vib}$ and $\bar{V}_m$ are the mean values of the atomic diameter, the melting enthalpy (H_m^{Nb}, H_m^{Cu}), vibrational part of the overall melting entropy ($S_{vib}^{Nb}, S_{vib}^{Cu}$) and the molar volumes (V_m^{Nb}, V_m^{Cu}) of corresponding substances consisting of interfaces, respectively. In Eq. (4), by taking the parameters [27,34]: $a_{Nb} = 4.08$ Å, $a_{Cu} = 2.9$ Å, $\mu_{Nb} = 3.75$ GPa, $\mu_{Cu} = 48.3$ GPa, $H_m^{Nb} = 26.4$ kJ/mol, $H_m^{Cu} = 13.1$ kJ/mol, $S_{vib}^{Nb} = 8.05$ J/(K mol), $S_{vib}^{Cu} = 8$ J/(K mol) $V_m^{Nb} = 10.87\ cm^3/mol$ and $V_m^{Cu} = 7.11\ cm^3/mol$, we can get $\Delta\gamma = -3.69\ J/m^2$. It means that some extra energy needs to achieve the phase transition from bcc-Nb to fcc-Nb by means of contracting the atomic diameter [27]. From thermodynamical point, it is unfavorable for the phase transition from bcc-Nb to fcc-Nb. However, it is possible to store excessive energy in Nb layers

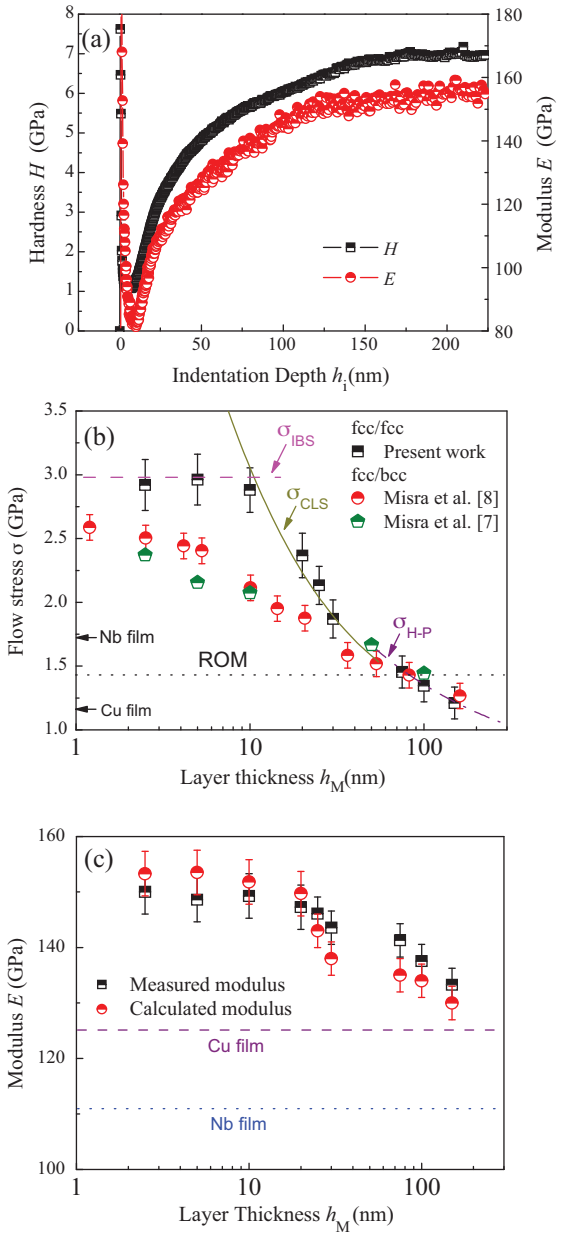

Fig. 3. (a) Plot of hardness vs. indentation depth and indentation modulus vs. indentation depth for Cu/Nb NMFs with $\lambda = 40$ nm plateaus are observed in both cases. (b) Dependence of flow stress on h_M for the Cu/Nb NMFs. The strength of Cu and Nb films is indicated by arrow, the rule of mixtures (ROM) estimates is indicated by dotted lines. In (b), the σ_{CLS}, σ_{IBS}, and σ_{H-P} are also presented. Misra et al.'s results [7,8] are also plotted for comparison. (c) Dependence of indentation modulus on h_M for the Cu/Nb NMFs. The modulus of Cu and Nb films are also shown (the horizontal dash line for Cu and dot line for Nb, respectively).

during the nonequilibrium deposition process by forming lots of defects such as vacancy and misfit dislocation, increasing free volume [35,36]. For example, in the immiscible system Ag/Nb with positive enthalpy of formation (~25 kJ/mol), amorphous alloy can be obtained during the nonequilibrium deposition [37].

3.2. Mechanical properties

The nanoindentation data were measured continuously during the loading of the indenter by the CSM method. Fig. 3(a) shows the variation in hardness and modulus with penetration depth for the fcc/fcc Cu/Nb NMFs with $\lambda = 40$ nm. We see that at small depths of indentation (<30 nm) the hardness falls with increasing depth, as expected on the basis of indentation size effects in bulk materials [38]. Then the hardness as well as the modulus starts to increase with increasing depth of indentation and saturates in the indentation depth range of ~100–225 nm (corresponding to ~15–40% of the multilayer thickness). Saha and Nix [38] pointed out that the effect of the substrate hardness on the film hardness was negligible in the case of soft films on hard substrates because the plastic deformation was contained within the film and the substrate yielded plastically only when the indenter penetrated the substrate. Hardness was observed to be constant for indentation depths less than the film thickness and these hardness plateaus to be good estimates of the true properties of the film [38]. Wen et al. [32] investigated the length scale-dependent hardness of Cu/W multilayers and demonstrated that the plateau value of measured hardness from a nanoindenter below 50% of the total film thickness is the intrinsic hardness of the multilayers. In our experiments, thus the hardness as well as the modulus determined as the average value from the plateau of hardness-indentation depth curve (the indentation depth range of ~100–225 nm) is reliable and reasonable. For comparison, the hardness and modulus of monolithic Cu and Nb films were also measured, and they are 3.46 GPa and 125 GPa for Cu film and 5.2 GPa and 112 GPa for Nb film, respectively. The flow stress (estimated as 1/3 of hardness) calculated from the rule of mixtures (ROM) for the composites is about $\sigma_{ROM} = 1.45$ GPa.

In Fig. 3(b), as h_M decreases from 150 to 10 nm, the flow stress of fcc/fcc Cu/Nb NMFs strongly increases first, and then reaches a plateau with h_M further decreases down to 2.5 nm. By contrast, the hardness of sputtered fcc/bcc Cu/Nb multilayers monotonically increases at this length scale (2.5–200 nm) [7,8]. The discrepancies between present fcc/fcc multilayers and sputtered fcc/bcc Cu/Nb [7,8] are probably caused by the differences in microstructure (e.g. grain size, lattice mismatch), deposition process, etc. Note that the maximum hardness achieved in present multilayers is significantly higher than the rule of mixtures estimates shown with dotted lines in Fig. 3(b). The deformation mechanism transition from dislocation gliding in the confined layer to dislocation cutting cross the interface, overcoming an additional resistance from the interface dislocation arrays is responsible for the saturation of the flow stress or hardness [8,39].

With regard to the metallic multilayers composed of a softer/ductile layer and a harder/brittle layer, plastic flow is controlled by the softer/ductile phase [13,14,29,40], i.e., the Cu layers. As the layer thickness $h_M \geq 75$ nm, the flow stress σ_{H-P} can be fitted well by H–P relationship [8]:

$$\sigma_{H-P} = \sigma_0 + k h_M^{-1/2} = 0.6 + 7.4 h_M^{-1/2}, \quad (5)$$

where σ_0 is a constant (~0.6 GPa) and contains contributions from lattice friction, grain boundary strengthening, etc.; h_M is the layer thickness; and k is the H–P slope (~7.4 GPa $\sqrt{\text{nm}}$) and can be given as [8]:

$$k = \sqrt{\frac{\tau^* \mu_{Cu} b_{Cu}}{\pi(1-\nu_{Cu})}}, \quad (6)$$

where τ^* is the barrier strength of interface for slip transmission; μ_{Cu} (48.3 GPa) is the shear modulus of Cu; b_{Cu} (0.2556 nm) is the magnitude of the Burgers vector of Cu and ν_{Cu} (0.343) is the Poisson ratio for Cu. Misra et al. [8] pointed out that the H–P slope k can be used to estimate the maximum strength σ_{IBS} ($\sigma_{IBS} = 3.06\tau^*$) of NMFs. According to Eq. (6), the σ_{IBS} of present fcc/fcc Cu/Nb NMFs is ~2.98 GPa by taking the parameters mentioned above and $k = 2.42$ GPa $\sqrt{\text{nm}}$ for a H–P fit to shear strength. It is consistent well with the measured peak strength ~2.88 GPa, see Fig. 3(b). At the H–P model applicable region, one can see that the $\sigma_{ROM} > \sigma_{H-P}$, which means the applied load is dominantly undertook by the Cu rather than the Nb. Compared with fcc/bcc Cu/Nb

NMFs with no significant difference between the grain sizes in the two phases [7,8], the (Nb) grain size effect is not the main reason for present fcc/fcc ones exhibited higher H–P slope. The larger δ is, the more pre-existing (misfit) dislocations at the interfaces. This can result in higher interface strengthening capability, due to more glide–interface interactions [3,39–41]. It is supported by the trend that present fcc/fcc Cu/Nb NMFs exhibits higher H–P slope ($k = 2.42\,\mathrm{GPa}\sqrt{\mathrm{nm}}$) than the fcc/bcc one ($k = 1.65$–$2.1\,\mathrm{GPa}\sqrt{\mathrm{nm}}$ [7,8]).

At the length scales where dislocation pile-up-based H–P model does not apply, the CLS model [8,39,40] involving the glide of single dislocation loop in soft phase bounded by two interfaces can be used to explain the increase in strength with decreasing h_M. Thus the CLS stress (σ_{CLS}) to generate a glide dislocation in the confined layer can be expressed as [8,29]

$$\sigma_{CLS} = \frac{M\mu^* b_{Cu}\ \sin\varphi}{8\pi h_M}\left(\frac{4-\nu_{Cu}}{1-\nu_{Cu}}\right)\ln\left(\frac{\alpha h_M}{b_{Cu}\ \sin\varphi}\right) - \frac{f}{h_M} + \frac{\mu^*\varepsilon}{2m(1-\nu_{Cu})}, \quad (7)$$

where M is the Taylor factor, ϕ is the angle between the slip plane and the interface, $\mu^* = (\mu_{Nb}\cdot\mu_{Cu})/(V_{Nb}\cdot\mu_{Cu} + V_{Cu}\cdot\mu_{Nb})$ is the shear modulus of Cu/Nb NMFs which can be estimated by the shear modulus μ_{Cu} and volume fraction V_{Cu} of the Cu layer and those of the Nb layer, α represents the core cut-off parameter, f is the characteristic interface stress of multilayer, ε is in-plane plastic strain and m is a strain resolution factor of the order of 0.41 for the active slip systems of fcc Nb, other symbols have the same meaning as mentioned above. The CLS model fits experimental data well as h_M decreases down to 10 nm by taking $M = 3.06$, $\alpha = 1$, $f = 3\,\mathrm{J/m^2}$, $\varepsilon = 1.2\%$ and $\phi = 70.5^\circ$ into Eq. (7), the dependence of σ_{CLS} on h_M is calculated and plotted in Fig. 3(b) as well. For present fcc/bcc Cu/Nb NMFs, the intersection point of the σ_{IBS} line and σ_{CLS} curve at about 2.98 GPa yields a critical $h_M^{cri}\sim$10 nm, consistent with the experimental data.

From Fig. 3(c), one can find that the modulus of fcc/fcc Cu/Nb multilayer remarkably increases with decreasing h_M from 150 down to 10 nm, and then almost reaches a plateau with further reducing h_M. The measured moduli of Cu/Nb NMFs are in agreement with the calculated ones according to Eq. (3) at a penetration depth of 125 nm, and much higher than those of monolithic Cu and Nb films. This can be considered as a modulus enhancement effect. At larger thickness ($h_M > 10$ nm), one can see the interface is sharp and no intermixing is observed. Hence, the compressed out-of-plane interplanar spacing of fcc Nb layer contributes the enhanced modulus. In contrast, at smaller layer thickness ($h_M < 10$ nm), the layer thickness is small and the deposition rate is fast ~0.6 nm/s, so that the Nb layers are not fully continuous and dense. Thus, Cu atoms are probably able to penetrate into the locations of incomplete coalescence to form some intermixing regions with the microstructure similar to amorphous between grain boundaries in Nb layers [32,37], even form some local intermixing region at interface during the sputtering process [2]. As to the modulus, amorphous regions play a negative role. It was reported that metallic glass has 1% larger specific volume ("free volume") than the crystalline state [42]. Free volume in the amorphous alloy regions has a negative contribution to the modulus, which results in a decrease of modulus with decreasing h_M because of more interfaces in the multilayers. Except the compressed out-of-plane interplanar spacing of fcc Nb layer, the small sized nanocrystalline Nb particles can also cause slight shrinkage of Nb (1 1 1) atomic planes due to the interface stress [37]. Both of the two effects can promote the enhancement of modulus. The competition between the factor reducing modulus and the factors increasing modulus probably results the measured modulus saturated at small layer thickness ($h_M < 10$ nm).

4. Conclusions

The Nb transformed from bcc to fcc structure was found in nanostructured Cu/Nb NMFs, which is analyzed by a thermodynamics model. At large length scale (layer thickness > 50 nm), the strength/hardness follows the H–P relationship; further reducing the length scale the strength/hardness obeys the CLS model. After that the saturation strength/hardness is attained, which is caused by dislocation cutting cross the interface. The fcc/fcc Cu/Nb NMFs exhibits higher strengthening ability than that of fcc/bcc Cu/Nb NMFs, due to the phase transition-induced larger lattice mismatch or higher (misfit) dislocation density at fcc/fcc interface. The enhanced modulus results from the compressed interplanar spacing of Nb layer.

Acknowledgements

This work was supported by the 973 Program of China (grant no. 2010CB631003), the 111 Project of China (B06025) and the National Natural Science Foundation of China (50971097). GL thanks the support of Fundamental Research Funds for the Central Universities, GJZ thanks the support of the Program for New Century Excellent Talents in University (grant no. NCET-10-0876) and JYZ thanks the financial support of China Scholarship Council (CSC).

References

[1] G.S. Was, T. Foecke, Thin Solid Films 286 (1996) 1.
[2] J.Y. Zhang, X. Zhang, R.H. Wang, S.Y. Lei, P. Zhang, J.J. Niu, G. Liu, G.J. Zhang, J. Sun, Acta Mater. 59 (2011) 7368.
[3] Y.P. Li, G.P. Zhang, W. Wang, J. Tan, S.J. Zhu, Scr. Mater. 57 (2007) 117.
[4] M.J. Demkowicz, R.G. Hoagland, J.P. Hirth, Phys. Rev. Lett. 100 (2008) 136102.
[5] N.A. Mara, D. Bhattacharyya, R.G. Hoagland, A. Misra, Scr. Mater. 58 (2008) 874.
[6] I. Bakonyi, L. Péter, Prog. Mater. Sci. 55 (2010) 107.
[7] A. Misra, H. Kung, Adv. Eng. Mater. 3 (2001) 217.
[8] A. Misra, J.P. Hirth, R.G. Hoagland, Acta Mater. 53 (2005) 4817.
[9] E.G. Fu, N. Li, A. Misra, R.G. Hoagland, H. Wang, X. Zhang, Mater. Sci. Eng. A 493 (2008) 283.
[10] J. McKeown, A. Misra, H. Kung, R.G. Hoagland, M. Nastasi, Scr. Mater. 46 (2002) 593.
[11] Y. Liu, D. Bufford, H. Wang, C. Sun, X. Zhang, Acta Mater. 59 (2011) 1924.
[12] P.M. Anderson, C. Li, Nanostruct. Mater. 5 (1995) 349.
[13] J.D. Embury, J.P. Hirth, Acta Metall. Mater. 42 (1994) 2051.
[14] M.A. Phillips, B.M. Clemens, W.D. Nix, Acta Mater. 51 (2003) 3157.
[15] J.S. Koehler, Phys. Rev. B 2 (1970) 547.
[16] S.I. Rao, P.M. Hazzledine, Philos. Mag. A 80 (2000) 2011.
[17] D. Van Heerden, D. Josell, D. Shechtman, Acta Mater. 44 (1996) 297.
[18] G.B. Thompson, R. Banerjee, S.A. Dregia, H.L. Fraser, Acta Mater. 51 (2003) 5285.
[19] R. Banerjee, X.D. Zhang, S.A. Dregia, H.L. Fraser, Acta Mater. 47 (1999) 1153.
[20] R. Banerjee, R. Ahuja, H.L. Fraser, Phys. Rev. Lett. 76 (1996) 3778.
[21] J. Chakraborty, K. Kumar, R. Ranjan, S.G. Chowdhury, S.R. Singh, Acta Mater. 59 (2011) 2615.
[22] H. Wormester, E. Huger, E. Bauer, Phys. Rev. Lett. 77 (1996) 1540.
[23] A.C. Redfield, A.M. Zangwill, Phys. Rev. B 34 (1986) 1378.
[24] R. Bruinsma, A.M. Zangwill, J. Phys. 47 (1986) 2055.
[25] S.A. Dregia, R. Banerjee, H.L. Fraser, Scr. Mater. 39 (1998) 217.
[26] G.B. Thompson, R. Banerjee, S.A. Dregia, M.K. Miller, H.L. Fraser, J. Mater. Res. 19 (2004) 707.
[27] J.C. Li, W. Liu, Q. Jiang, Acta Mater. 53 (2005) 1067.
[28] J.Y. Zhang, G. Liu, X. Zhang, G.J. Zhang, J. Sun, E. Ma, Scr. Mater. 62 (2010) 333.
[29] J.Y. Zhang, X. Zhang, G. Liu, G.J. Zhang, J. Sun, Scr. Mater. 63 (2010) 101.
[30] J.Y. Zhang, X. Zhang, G. Liu, G.J. Zhang, J. Sun, Mater. Sci. Eng. A 528 (2011) 2982.
[31] M.F. Doerner, W.D. Nix, J. Mater. Res. 1 (1986) 601.
[32] S.P. Wen, R.L. Zong, F. Zeng, Y. Gao, F. Pan, Acta Mater. 55 (2007) 345.
[33] J. Häglund, A. Fernández Guillermet, G. Grimvall, M. Körling, Phys. Rev. B 48 (1993) 11685.
[34] M. Sasaki, M. Koyano, H. Negishi, M. Inoue, Thin Solid Films 158 (1988) 123.
[35] P.P. Chattopadhyay, P.M.G. Nambissan, S.K. Pabi, I. Manna, Phys. Rev. B 63 (2001) 054107.
[36] P.P. Chatterjee, S.K. Pabi, I. Manna, J. Appl. Phys. 86 (1999) 5912.
[37] W.S. Lai, M.J. Yang, Appl. Phys. Lett. 90 (2007) 181917.
[38] R. Saha, W.D. Nix, Acta Mater. 50 (2002) 23.
[39] A. Misra, J.P. Hirth, H. Kung, Philos. Mag. A 82 (2002) 2935.
[40] J.Y. Zhang, S. Lei, Y. Liu, J.J. Niu, G. Liu, X. Zhang, J. Sun, Acta Mater. 60 (2012) 1610.
[41] D. Saraev, R.E. Miller, Acta Mater. 54 (2006) 33.
[42] A. Van Den Beukel, S. Radelaar, Acta Metall. 31 (1983) 419.